CrossMark

Chemical functionalization of graphene oxide and its electrochemical potential towards the reduction of triiodide

Syeda Qudsia[1] · Muhammad Imran Ahmed[1] · Zakir Hussain[1] · Shahid Soomro[2]

Abstract Among a diverse set of properties, graphene is also noted for its electrochemical and catalytic capabilities. These can also be influenced by functionalization of graphene. This study reports the chemical functionalization of graphene oxide (GO) with an aromatic compound 4-hydroxy-4′-n-pentylbiphenyl, by an esterification reaction. Formation of new coupled product was investigated through scanning electron microscopy, X-rays diffractometer, Fourier-transform infrared, and UV–Vis spectrometry studies. UV–visible spectrometry also indicated an increase in band gap energy, likely due to the Burstein–Moss effect. Electrochemically, the esterified product was found to be better than GO in terms of triiodide reduction, which gives plausible worth to exploring this functionalization strategy further for the development of counter electrode materials for dye-sensitized solar cells.

1 Introduction

Graphene was discovered in a Nobel-winning experiment in 2004 and since then, it has been the center of attention of a large number of studies [1]. The material characteristics, such as huge surface area, outstanding mechanical strength, ~97% optical transparency, excellent electronic-transport and thermal conductivityare a few among many of its remarkable properties [1–5]. This makes it an attractive material for research and its potential use is expected to be a life-changer for a variety of applications, such as electronic devices, sensing applications, energy generating and storage applications and in biomedicine and biotechnology [6–14].

Graphene and related materials, such as graphene oxide (GO), have also been explored for their electrochemical catalytic activity in various systems [15, 16]. In numerous studies, it has been conjugated or functionalized with other materials for improvement in performance [17, 18]. There are two basic functionalization schemes for graphene: chemical functionalization bycovalent linkages, or physical coupling via π–π interactions [19]. Researchers have reported functionalization of graphene with various moieties, ranging from small organic molecules and polymers to nanoparticles and even biomaterials for desired properties and applications [18]. Composites of the kind have been tested for their capability for oxygen reduction, glucose oxidation, hydrogen peroxide reduction and reduction of industrial chemicals [20–25].

One burgeoning area that graphene and its conjugates have found is the electrochemical reduction of triiodide to iodide in photoelectrochemical systems known as dye-sensitized solar cells (DSSCs) [16, 26]. DSSCs employ a nanoporous layer of titanium dioxide, sensitized with an organic dye [26]. This 'photoanode' is a part ofsandwich-type cell filled with an electrolyte containing a redox couple, mainly iodide/triiodide [26]. The dye, excited by photo irradiation, injects an electron into the conduction band of titania [26]. When this electron re-enters the cell at the cathode, or counter electrode, platinum catalyst helps in the reduction of triiodide to iodide, which in turn helps in the regeneration of the oxidized dye to maintain performance of a DSSC [26, 27]. Platinum catalysts have high costs and are

✉ Zakir Hussain
  zakir.hussain@scme.nust.edu.pk

[1] School of Chemical and Materials Engineering (SCME), National University of Sciences & Technology (NUST), Sector H-12, Islamabad 44000, Pakistan

[2] Bremer Pharma GmBH, Werkstr. 42, 34414 Warburg, Germany

susceptible to poisoning by the electrolyte, hence a number of alternatives are being experimented upon, which include carbon compounds [28]. In the past, carbon black and graphite powders have been found to make for stable catalytic counter electrodes due to their porous structures and roughness [28]. Carbon nanotubes have also been exploited for the purpose and their performance has been found to be dependent on layer thickness and defects density [29].

GO has also been used as the catalytic counter electrode and its performance have been found to be comparable to platinum catalysts, with more defects and oxygen functionalities aiding the catalytic activity [30]. Excellent performance has also been reported for thermally reduced GO [31]. Counter electrodes based on exfoliated graphene sheets have demonstratedan efficiency that is 0.8 times compared to cells with platinum based counter electrodes [32]. Graphene sheets have also been oriented in a vertical manner to expose more edges at the surface for improvement in catalytic performance, as edges are believed to provide the active sites for catalysis [33, 34].

A variety of modifications have also been studied in this regard which report a positive effect on the catalytic activity of graphene and GO. The incorporation of nitrogen atoms into carbon networks can significantly improve their electric and reactive properties, which is particularly important in catalysis due to the creation of new active sites [35]. Graphene has also been functionalized with nitric acid, and fluorine atoms, that has led to composites with better reaction kinetics [36, 37]. Surface functionalized GO with polyelectrolytes has been carried out for modulation of their catalytic activity towards triiodide species in a DSSC [31, 38]. Non-covalent functionalization with polymers like polypyrrole and covalent attachment with PEDOT-PSS and PVP have also been described as counter electrode materials fulfilling the same purpose [39–41]. Increased electrocatalytic performance of GO is attributed tobetter conductivity of composites; introduction of a positive charge that attracts negatively charged triiodide;surface area, morphology of graphene film, and the presence of defects and functional groups, which provide additional active sites for catalysis [30, 31, 38–42].

In this study, we report the chemical functionalization of GO to 4-hydroxy-4′-n-pentylbiphenyl (HPBP) via an esterification reaction. The product was analyzed, structurally, chemically and optically for confirmation of covalent grafting of both molecules. It was further investigated for its electrochemical performance through cyclic voltammetry (CV) and electrochemical impedance spectroscopy (EIS) for potential application as a catalytic counter electrode in DSSCs. We expected that the two-ring structure of HPBP would impact the electron cloud of GO and would change its optical and catalytic behavior and may prove to be a better alternative than GO for the aforementioned application.

To the best of our knowledge this is the first report investigating the chemical functionalization of GO with HPBP for application as a counter electrode in DSSCs.

2 Experimental

2.1 Materials and methods

Single layer GO was purchased from Graphene Supermarket, US. *N, N′*-Dicyclohexylcarbodiimide (DCC) and 4-dimethylaminopyridine (DMAP) were used as catalysts in the esterification reaction and were both from Sigma Aldrich (98%). The solvent employed for esterification reaction was dimethyl sulfoxide (DMSO), (Daejung, 99.5%). 4-hydroxy-4′-n-pentylbiphenyl (MIS Scientific, China, 98%)molecule was used for the functionalization of GO sheets. Indium tin oxide (ITO) coated glass substrates (resistance <7 Ω/cm^2) were used for optical profilometry, CV, and EIS. Iodide/triiodide electrolyte for electrochemical studies was from Solaronix SA, Switzerland while Pt coated glass were from Solaronix SA, Switzerland.

2.2 Functionalization of graphene oxide (GO)

GO was functionalized by esterification, based on the protocol mentioned by Gan et al., 2015 [43]. Briefly, 0.05 g (50 mg) of GO was suspended in 10 mL DMSO and sonicated for 90 min. It was then poured into a round bottom flask and set to stirring for another 30 min. DCC (2.0 g) and DMAP (1.7 g) were added to this mixture and stirring was continued for 30 min. Subsequently, 0.007 g (7 mg) of HPBP was dissolved in 10 mL DMSO and poured into the stirring mixture. Reaction mixture was stirred under inert atmosphere (argon) for 4 days at 60 °C. Finally, the reaction was quenched by the addition of 200 mL of methanol, divided into 15 mL falcon tubes and centrifuged at 4000 rpm for 3 h. The supernatant was discarded and the mixture was washed with acetone followed by washing with hot water (thrice, ~60 °C). The esterified product was dried overnight at 60 °C and named as GO-R (Fig. 1).

2.3 Sample preparation for electrochemical studies

Fresh ITO glass slides were washed with mild soap solution (sonicated for 10 min) followed by successive washings in distilled water (5 min + 5 min), acetone (10 min) and distilled water (5 min + 5 min). GO and GO-R suspensions were prepared in DMSO (0.5 mg/mL) and sonicated for 90 min. 20 μL of the suspension was drop casted on the conductive side of ITO glass (two slides each for GO and GO-R), leaving a 0.2 mm strip on each slide for electrical contacts during measurements. The slides were dried
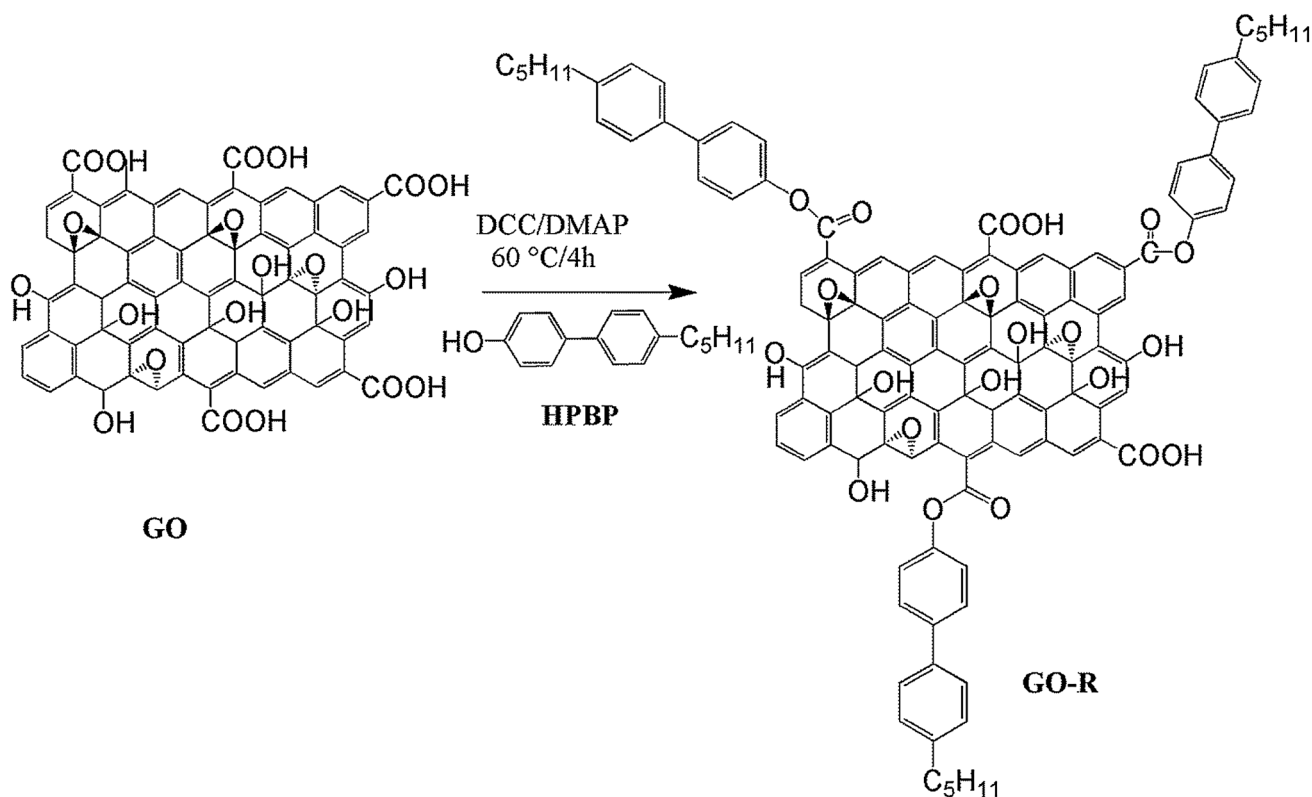
Fig. 1 Reaction scheme for the esterification of graphene oxide (GO) to GO-R

overnight at 50 °C. Two platinum coated glass slides were also washed according to the protocol mentioned above. These were then dried and fired at 400 °C for an hour in a blastfurnace.

Paraffin film spacers were prepared with a negative area of 0.8 cm × 1 cm. These were centered on one of the slides and a drop of iodide/triiodide electrolyte was placed in the center. The other slide of the pair was clamped on top with binder clips holding the assemblage. Four such sandwich cells were prepared, namely an ITO blank cell, a Pt-Glass cell, and GO-ITO and GO-R-ITO cells. Effective cell area was 0.8 cm^2.

2.4 Characterization

SEMof GO and GO-R (ultra-pure water based) was performed on JEOL JSM 6490 (LA) at an acceleration voltage of 20 kV.STOE Powder X-rays diffractometer was used for recording XRD results of dry sample powders with Cu K$_\alpha$ radiation (λ = 0.154 nm) from 5° to 80° (2θ). Powdered samples were incorporated into a KBr pellet and spectra were recorded between 4000 and 400 cm^{-1} wavenumbers for FT-IR spectroscopy (PerkinElmer spectrum 100). Samples for UV–Vis spectrophotometry were prepared in DMSO for HPBP and ultra-pure water for GO and GO-R

and were measured using T-60 UV–Vis spectrophotometer (PG Instruments), with a wavelength sweep from 1100 to 200 nm. Optical profilometer utilized for calculating the roughness and thickness of the sample coated on glass slides was from Nanovea (Model PS50). Electrochemical studies, CV and EIS were carried out on a multipotentiostat (BioLogicVSP system), using sandwich cells prepared as mentioned in Sect. 2.3. CV analysis was carried out from +1.0 to −1.0 V with a scan rate of 100 mV/s. EIS measurements were recorded in a frequency range of 1–400 kHz with a 10 mV magnitude of alternating signal. Z-Fit in EC lab software (version 10.40) was used for fitting of EIS data.

3 Results and discussion

3.1 Visual inspection and microscopy

GO formed a dark brown colored suspension which was miscible in common hydrophilic solvents. After esterification, it transformed to a much darker, blackish shade which was observed to form less stable dispersions in water, ethanol, and acetone but partially stable suspensions in DMSO under extended sonication. Since structure of HPBP shows

that it is relatively hydrophobic in nature, when hydroxyl groups of HPBP react with carboxylic acid groups of GO to form ester bonds, hydrophilicity of GO reduces [44]. Hence, above behavior regarding dispersion of final product in various solvents may have originated from the surface functionalization of GO.

SEM micrographs are shown in Fig. 2, where (a) depicts GO before esterification reaction and (b) shows the esterified GO i.e. GO-R. SEM results do not visually show any remarkable change in morphology of GO, but it can be seen that while GO shows well-adhering, spread out sheets, GO-R forms flakes that stand out from the background, likely as an effect of edge-functionalization of hydrophilic GO sheets with hydrophobic HPBP moiety. On the basis of the clear micrograph of functionalized conjugate at ×3700 magnification in the (b), it may also be safely assumed that functionalization caused aggregation of sheets to some extent, due to the incompatible nature of the GO sheet and HPBP, to achieve a stable, lowest energy orientation.

3.2 X-ray diffraction

GO displays a single peak at 9.6° representing reflection from 001 plane. Based on Braggs law, *d*-spacing is calculated to be 0.91 nm. In the case of functionalized compound, we observe that the peak for GO disappears and two other peaks appear instead, at 7.5° and 10.4°, equating to a *d*-spacing of 1.16 and 0.84 nm, respectively. GO-R further exhibits four prominent peaks, at 17.2°, 20.1°, 21.7°, and 44.1°. Although changes in the morphology of the sheets were not detected in SEM micrographs, these additional peaks in XRD show that functionalization induced molecular changes in the synthesized conjugate which differed significantly from GO with respect to its structural conformation (Fig. 3).

3.3 Fourier transform infrared (FT-IR) spectroscopy

FT-IR show peaks typical for GO at 3388 cm^{-1} corresponding to the presence of hydroxyl groups, 1739 cm^{-1} peak representing the stretching vibrations of C═O of the carboxylic acid group [45]. Absorption at 1613 cm^{-1} can be
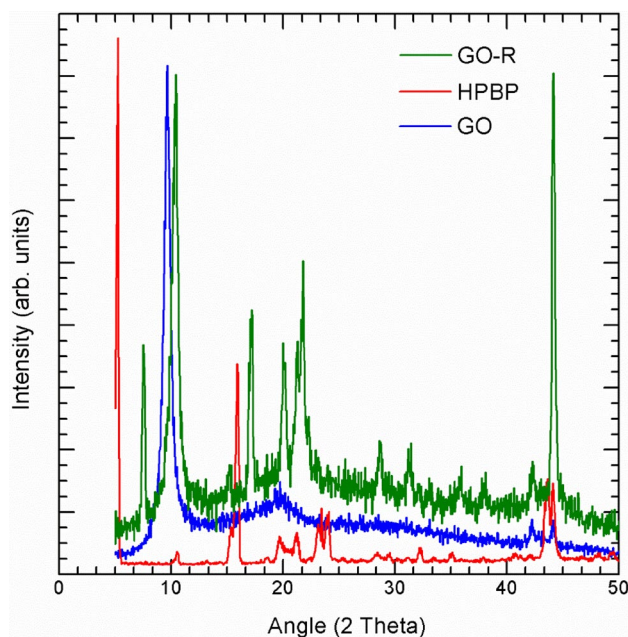
Fig. 3 XRD results of GO, GO-R and HPBP indicating a typical peak of GO at 9.6° (2θ), while number of peaks for GO-R that do not show up in either GO or HPBP, indicating the formation of a significantly different structure
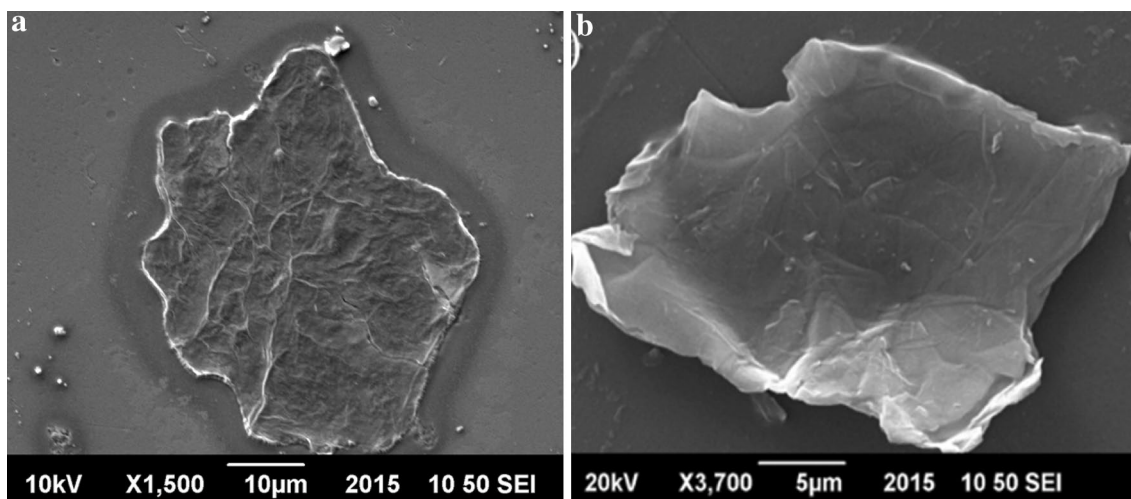
Fig. 2 Scanning electron micrographs of **a** graphene oxide (GO) and **b** esterified graphene oxide (GO-R)

attributed to the vibrations of aromatic rings of graphene backbone [46]. The peak around 1200 cm^{-1} shows the stretching vibrations of C–OH bond [46]. Deformation of the C–O bond can be linked with the intense band at 1050 cm^{-1} [45].

After functionalization, coupled product showed significant differences in FT-IR spectra, representing the successful chemical functionalization of GO (Fig. 4). The appearance of two peaks at 2900 cm^{-1} (–CH–stretching vibration) indicated that the resulting product contained more CH groups [43]. The broad nature of OH absorption observed at 3388 cm^{-1} also decreased in its intensity. The considerably diminished peak at 1739 cm^{-1} combined with absorption at 1246 cm^{-1} can be attributed to the C=O and C–O stretching of the ester bond [46].

3.4 UV–Vis spectrophotometry

UV–Vis spectrophotometry was performed to calculate the band gap of the material by cut-off method and to determine the amount of conjugation and electron delocalization in the GO and coupled product. In this case, λ_{max} indicates the degree of oxidation or reduction of GO. Therefore, in our case, GO shows a broad absorption peak with a λ_{max} of 235 nm. The shoulder around 300 nm indicates the n→π* transitions of the carbonyl groups present in GO [47].

In the case of functionalized compound, two absorption maxima were observed; the first peak has a maximum absorption at 278 nm while the second peak falls into the extreme UV range (or lies blue-shifted to the original absorption peak of GO). First peak is assumed to be due to the presence of HPBP moiety while the original peak of GO is also blue-shifted [48]. Such electronic changes in the band structure of the coupled product could be attributed to the Burstein–Moss effect which propose that electron withdrawal leads to occupation of electronic states in the conduction band and consequently to an increase in Fermi level and band gap energy [49]. This behavior is further supported by the better electrochemical performance of our coupled product which attracts triiodide more efficiently towards its surface [31, 38]. A blue-shift in the cut-off wavelength value is also observed for the first peak of GO-R (compared to HPBP). These shifts indicate that after covalent functionalization, two compounds interacted with each other at the molecular and electronic level, observed through shifting of absorbance in the given spectra (Fig. 5).

The band gap energy of the compounds was also calculated by the cut-off method, using the equation:

$$E = \frac{h \cdot c}{\lambda}$$

where h is the Planck's constant (6.626×10^{-34}), c is the speed of light (3×10^8 ms^{-1}), and λ is the cut-off wavelength recorded by taking the x-intercept at the point of increasing absorption with respect to the baseline. HPBP compound gave a cut-off value of 338 nm and the first
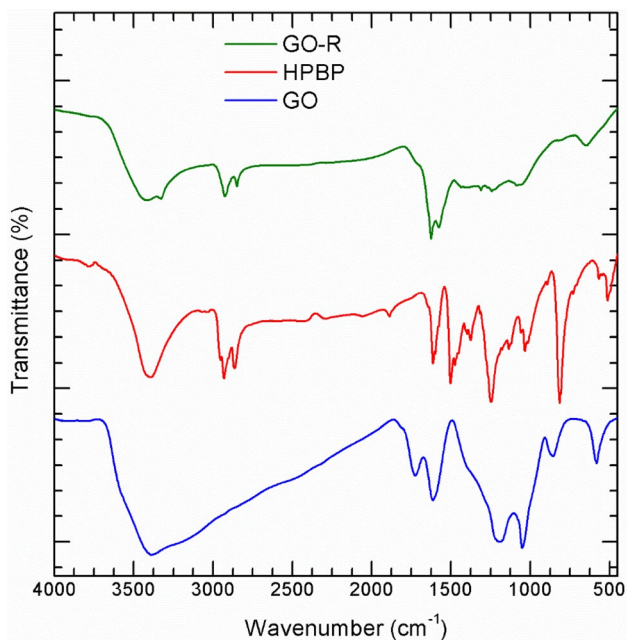
Fig. 4 FT-IR spectra of GO, GO-R and HPBP. Results confirm the formation of ester bonds between GO and HPBP
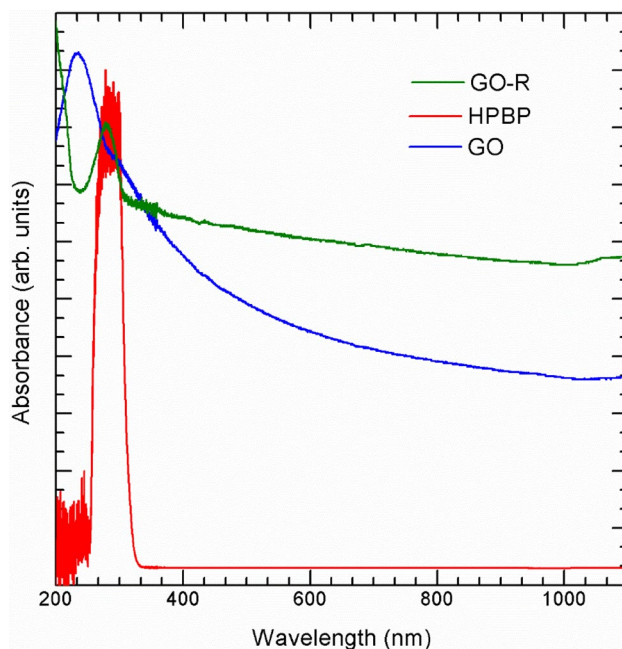
Fig. 5 UV–Vis spectra of GO, GO-R and HPBP. GO and HPBP show absorption maxima at 235 and 278 nm respectively while GO-R shows two peaks, one at 278 nm the other blue-shifted to the original GO peak

Table 1 Band gap energies for the GO, GO-R and HPBP compounds

Sample	λ_{max} (nm)	Cut-off λ (nm)	Band gap energy E (eV)
GO	235	–	–
GO-R	278	314	3.956
HPBP	278	338	3.675

Table 2 Values for arithmetic average roughness (R_a) and root mean square roughness (R_{rms}) obtained through optical profilometry

Sample	R_a (nm)	R_{rms} (nm)
ITO	4947	7256
GO	7127	10,475
GO-R	339	1035

peak of GO-R gave cut-off at 314 nm, which gives a band gap energy of 3.675 eV for HPBP and 3.956 eV for GO-R (Table 1).

3.5 Optical profilometry

To gauge the roughness factor and whether it has an effect on the electrocatalytic performance of GO and GO-R, we conducted optical profilometry of the samples which were drop casted on ITO electrodes and dried overnight at ambient temperature (Table 2). It can be seen from the

arithmetic average roughness value (R_a) and root mean square roughness (R_{rms}) that while GO had considerable roughness as compared to bare ITO glass; the esterified conjugate gave a much lesser value. Therefore, in the present study, surface roughness has not been considered in the final interpretation of electrocatalytic activity of GO and GO-R compounds.

3.6 Electrochemical behavior

The electrochemical performance of the material was measured through CV and EIS in a symmetric cell with an iodide/triiodide electrolyte. CV was performed from −1.0 to 1.0 V at a scan rate of 100 mV/s. Difference in volts between the oxidation and reduction peaks of a reaction (E_{pp}) and the current density exhibited by the compound (I_p) are the factors that are important in determining the catalytic activity of a material with respect to CV. Generally, two pairs of oxidation and reduction peaks appear for iodide/triiodide redox couple, corresponding to the redox reactions between I_2/I_3^- and I^-/I_3^-. Although in the present case, peaks (Fig. 6) did not achieve much resolution, however, it is apparent that the current at platinum electrodes started to climb much earlier followed by the coupled product, GO and ITO samples. It is also evident from the graphs that the platinum electrode showed the highest current density. However, among the other three compounds, coupled product exhibited a greater current density compared to GO and bare ITO slides. Therefore, coupled product assumed
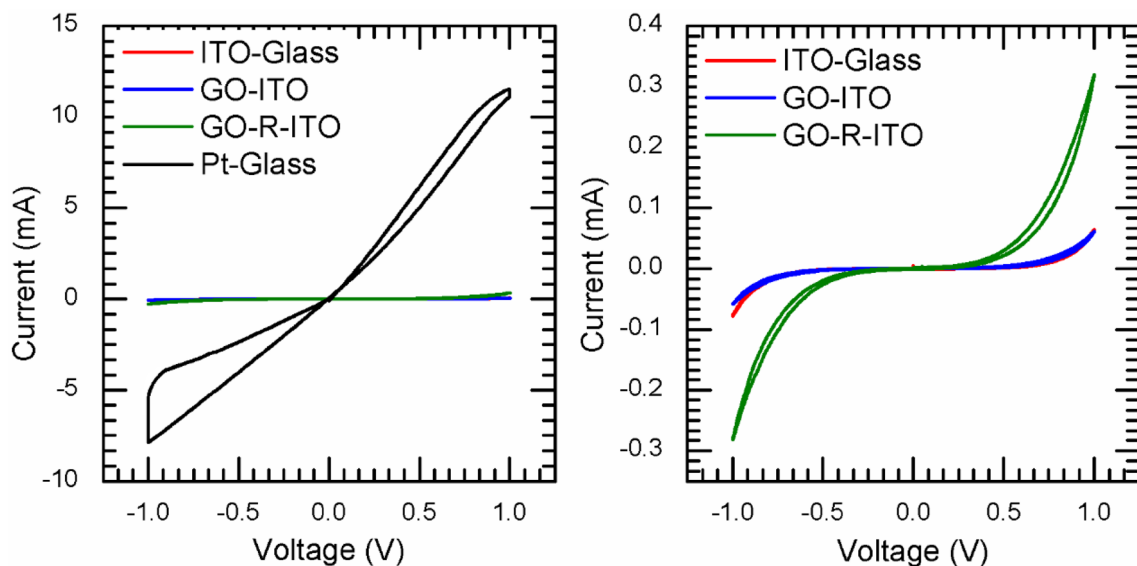

Fig. 6 CV results shown for platinum on glass, ITO glass, GO coated on ITO glass, and functionalized compound, GO-R, coated on ITO glass. The *right-hand side* graph shows the same results, but without those of platinum cells. Platinum gives the highest current density

among all four, corresponding to the least charge transfer resistance (R_{ct}) while GO-R comes second followed by the current densities for GO and ITO

to showa better catalytic activity as compared to either GO or ITO, also reflected from EIS data.

EIS measurements were recorded for the same symmetric cells, having iodide/triiodide electrolyte, and were recorded over a frequency range of 400–1 Hz with avoltage amplitude of 10 mV. The data obtained wereanalyzed using Zfit in EC-Lab V10.40 software, with Randomize+Levenberg–Marquardt algorithm (randomization was stopped at 10,000 iterations and fit was stopped at a relative error of $1e^{-6}$). A simple Randles circuit (Fig. 7) was used as an equivalent circuit for the fit. A Warburg impedance element was employed in series with the charge transfer resistance (R_{ct}) and a constant phase element (CPE) was used instead of an ideal capacitor for a better fit.

The data were plotted in the form of a Nyquist plot (Fig. 8), representing a complex plane with the imaginary y-axis encompassing values for the capacitive component
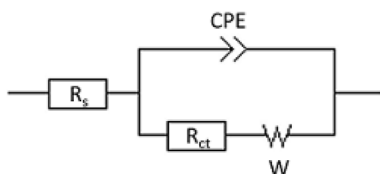

Fig. 7 The equivalent circuit employed for fitting of EIS data

of impedance and x-axis describing the resistive parameter. Each dot on the complex plot is obtained from information gained at a particular value of frequency during the frequency sweep, with the dot closest to the origin representing data recorded at the highest frequency. Magnitude of impedance increases with lowering frequency.

Typically, EIS results for symmetric cells show two to three semi-circles: the high frequency region is specific to the RC network at the interface, and the semi-circle at this end is attributed to the charge transfer processes [31, 50]. Between 0.1 and 10 Hz, impedance refers to the diffusion impedance called the Warburg impedance, which arises from mass transport limitations due to diffusion in the electrolyte [29, 50]. The series resistance at higher frequencies, where the phase difference is zero, shows the total resistance of the external circuit, including wiring and resistance of transparent electrodes, and resistance imposed by the liquid electrolyte in bulk [29]. The series resistance can be calculated by taking the x-intercept of the plot at the high frequency end.

In our case, the semi-circles expected in the Nyquist plots failed to resolve clearly and the response obtained could be approximated to a straight line. A linear correlation between real and imaginary impedance in such a graph may depict a diffusion-limited process with facile electron transfer [51]. A vertical line along the x-axis describes

Fig. 8 Nyquist Impedance plots for Pt-Glass, ITO-Glass, GO-ITO-Glass, and GO-R-ITO-Glass with real, *x-axis* representing the resistive parameter, and imaginary impedance, or the capacitive component of impedance, plotted on *y-axis*
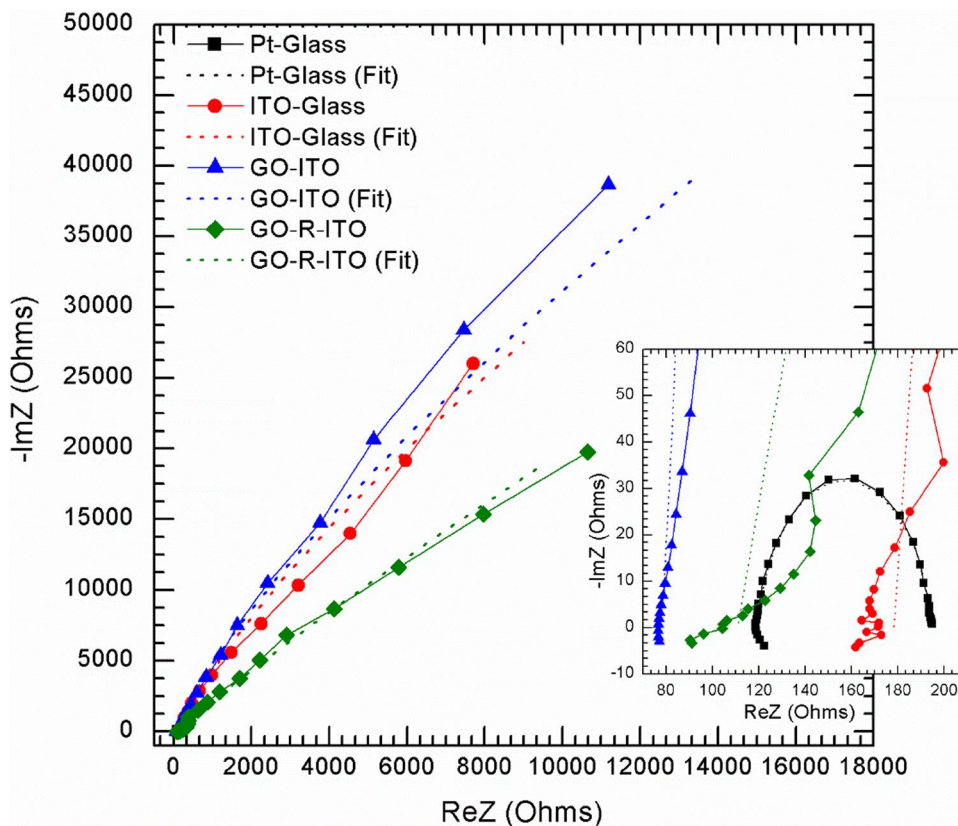
an ideal capacitance, and the closer the line is to a phase shift of 90°, the more ideal the capacitance is considered and less charge transfer is expected [52, 53]. Cheng et al. have described the slope of this line as a representation of the diffusion resistance within the porous network of the electrode and the sample material, with an increase in slope depicting lowered diffusion resistance within the material [52]. In a previous study with multi-walled carbon nanotubes, a straight line obtained for catalytic activity was resolved into three semi-circles as sample deposition was increased as a function of time [54]. Therefore, it can be inferred that increasing sample loading on the electrodes would alter the electrochemical response and can be explored in future.

Charge transfer resistance is a measure of the catalytic activity of the counter electrode. In our case, platinum-gave the best performance with a charge transfer resistance of 75.17 Ω and a series resistance, corresponding to the resistance of the external circuit and liquid electrolyte, was found to be ~122 Ω. Compared to Pt-Glass, ITO-Glass had a much higher charge transfer resistance of 45.9 kΩ. However, upon coating the ITO-Glass with GO and functionalized GO samples, there was a remarkable reduction in charge transfer resistance from 45.9 to 7.8 kΩ in the case of GO and down to only ~2.9 kΩ in the case of functionalized GO (GO-R). This can be attributed to better conductivity of GO-R sample also evident from CV results (Table 3).

In the case of series resistance, the symmetric cells with GO electrodes showed the least resistance of ~77 Ω which slightly increased for the GO-R (~90 Ω). Series resistance is affected by conductivity of the material, inter-particle resistance and contact resistance between ITO and GO, and hence, might indicate less contact resistance between GO sheets and ITO as compared to the GO-R [52]. While GO-R showed a considerable decrease in charge transfer resistance compared to its GO counterpart; GO was found to have a better circuit resistance value, likely due to the lowered contact resistance between GO sheets and ITO surface.

Table 3 Data on the electrochemical behavior of various samples

Sample	EIS		CV	
	R_s (Ω)	R_{ct} (Ω)	$I_{p\,Red}$ (mA)	$I_{p\,Ox}$ (mA)
Pt-glass	122.1	75.17	−4.284	11.096
ITO-glass	161.6	45,914	−0.077	0.064
GO-ITO-glass	77.0	7866	−0.058	0.060
GO-R-ITO-glass	90.9	2989	−0.281	0.320

Values obtained for series resistance and charge-transfer resistance for each sample after fitting with equivalent circuit. Maximum current density recorded through CV measurements is also included

4 Conclusions

In this study, we show the covalent edge-functionalization of GO and its electrochemical performance in terms of trii-odide reduction for its potential use as counter electrode material in a DSSC device. While much change in morphology was not observed, FTIR and XRD results showed the formation of ester bonds and the consequent synthesis of a new compound with differing structural characteristics. UV–Vis spectrophotometry showed two distinct peaks, one arising from HPBP compound and the other from GO, with a blue-shift attributed to the Burstein–Moss effect. The esterified compound showed a better electrocatalytic activity as compared to regular GO and blank ITO glass slides, which may be attributed to its higher conductivity, clearly observable in cyclic voltammograms. Thus behavior can be attributed to the presence of HPBP on the basal plane of GO with a relatively low electronic density and serving as meansfor electrostatic attraction towards negatively charged triiodide molecules, and hence resulted in better electron transfer kinetics. In future, we hope to further explore the effect of functionalization of GO with ringed structures on its electrochemical behavior and develop materials that can be used as the catalytic counter electrode in DSSC devices.

References

1. K.S. Novoselov, A.K. Geim, S.V. Morozov, D. Jiang, Y. Zhang, S.A. Dubonos, I.V. Grigorieva, A.A. Firsov, Science **306**, 666 (2004)
2. S. Stankovich, D.A. Dikin, G.H. Dommett, K.M. Kohlhaas, E.J. Zimney, E.A. Stach, R.D. Piner, S.T. Nguyen, S.R. Ruoff. Nature **442**, 282 (2006)
3. C. Lee, X. Wei, J.W. Kysar, J. Hone, Science **321**, 385 (2008)
4. R.R. Nair, P. Blake, A.N. Grigorenko, K.S. Novoselov, T.J. Booth, T. Stauber, N.M.R. Peres, A.K. Geim, Science **320**, 1308 (2008)
5. A.A. Balandin, S. Ghosh, W. Bao, I. Calizo, D. Teweldebrhan, F. Miao, C.N. Lau, Nanoletters, 8, 902 (2008)
6. M.D. Stoller, S. Park, Y. Zhu, J. An, R.S. Ruoff, Nanoletters, 8, 3498 (2008)
7. M. Burghard, H. Klauk, K. Kern, Adv. Mater. **21**, 2586 (2009)
8. S. Alwarappan, A. Erdem, C. Liu, C.Z. Li, J. Phys. Chem. C **113**, 8853 (2009)
9. Y. Wang, Y. Li, L. Tang, J. Lu, J. Li, Electrochem. Commun. **11**, 889 (2009)
10. Y. Shao, J. Wang, H. Wu, J. Liu, I.A. Aksay, Y. Lin, Electroanalysis, 22, 1027 (2010)
11. Y. Liu, Y. Liu, H. Feng, Y. Wu, L. Joshi, X. Zeng, J. Li, Biosens. Bioelectron. **35**, 63 (2012)
12. D.A. Brownson, D.K. Kampouris, C.E. Banks, J. Power Sour. **196**, 4873 (2011)

13. C. Hu, L. Song, Z. Zhang, N. Chen, Z. Feng, L. Qu, Energy Environ. Sci. 8, 31 (2015)
14. Z. Liu, J.T. Robinson, X. Sun, H. Dai, J. Am. Chem. Soc. **130**, 10876 (2008)
15. Z. Yang, H. Nie, X.A. Chen, X. Chen, S. Huang. J. Power Sour. **236**, 238 (2013)
16. D. Deng, K.S. Novoselov, Q. Fu, N. Zheng, Z. Tian, X. Bao, Nat. Nanotechnol. **11**, 218 (2016)
17. P. Lü, Y. Feng, X. Zhang, Y. Li, W. Feng, Sci. China Technol. Sci., 53, 2311 (2010)
18. D. Chen, H. Feng, J. Li, Chem. Rev. **112**, 6027 (2012)
19. Y. Hu, X. Sun, In Advances in Graphene Science, ed. by M. Ali-ofkhazraei, InTech, Rijeka, Croatia (2013)
20. Y. Wang, J. Lu, L. Tang, H. Chang, J. Li, Anal. Chem. **81**, 9710 (2009)
21. S. Wang, D. Yu, L. Dai, D.W. Chang, J.B. Baek, ACS Nano **5**, 6202 (2011)
22. T. Gao, D. Yang, L. Ning, L. Lei, Z. Ye, G. Li, Nanoscale **6**, 14828 (2014)
23. C.K. Chua, M. Pumera, ACS Nano **9**, 4193 (2015)
24. M. Liu, R. Liu, W. Chen, Biosens. Bioelectron. **45**, 206 (2013)
25. X. Gao, G. Xu, Y. Zhao, S. Li, F. Shi, Y. Chen, RSC Adv. 5, 88045 (2015)
26. B.O'Regan, M. Grätzel, Nature **353**, 737 (1991)
27. M.K. Nazeeruddin, A. Kay, I. Rodicio, R. Humphry-Baker, E. Müller, P. Liska, N. Vlachopoulos, M. Grätzel, J. Am. Chem. Soc. **115**, 6382 (1993)
28. A. Kay, M. Grätzel, Sol. Energy Mater. Sol. C, 44, 99 (1996)
29. J.E. Trancik, S.C. Barton, J. Hone, Nanoletters 8,982 (2008)
30. J.D. Roy-Mayhew, D.J. Bozym, C.A. Punckt, C.I. Aksay, ACS Nano **4**, 6203 (2010)
31. P. Hasin, M.A. Alpuche-Aviles, Y. Wu, J. Phys. Chem. C **114**(37), 15857 (2010)
32. A. Kaniyoor, S. Ramaprabhu, In 2011 International conference on nanoscience, technology and societal implications (NSTSI) (IEEE, 2011) pp1
33. X. Pan, K. Zhu, G. Ren, N. Islam, J. Warzywoda, Z. Fan, J. Mater. Chem. A **2**, 12746 (2014)
34. P.M. Hallam, C.E. Banks, Electrochem. Commun. **13**, 8 (2011)
35. G. Wang, W. Xing, S. Zhuo. Electrochim. Acta **92**, 269 (2013)
36. S. Das, P. Sudhagar, V. Verma, D. Song, E. Ito, S.Y. Lee, Y.S. Kang, W. Choi, Adv. Funct. Mater. 21, 3729 (2011)
37. S. Das, P. Sudhagar, E. Ito, D.Y. Lee, S. Nagarajan, S.Y. Lee, Y.S. Kang, W. Choi, J. Mater. Chem. **22**, 20490 (2012)
38. A. Kaniyoor, S. Ramaprabhu, J. Mater. Chem. **22**, 8377 (2012)
39. W. Liu, Y. Fang, P. Xu, Y. Lin, X. Yin, G. Tang, M. He, ACS Appl. Mater. Interfaces **6**, 16249 (2014)
40. W. Hong, Y. Xu, G. Lu, C. Li, G. Shi, Electrochem. Commun. **10**, 1555 (2008)
41. Z.Y. Li, M.S. Akhtar, J.H. Kuk, B.S. Kong, O.B. Yang, Mater. Lett. **86**, 96 (2012)
42. C. Punckt, M.A. Pope, J. Liu, Y. Lin, I.A. Aksay, Electroanalysis 22, 2834 (2010)
43. L. Gan, S. Shang, C.W.M. Yuen, S. X. Jiang, RSC Adv. 5, 15954 (2015)
44. H. He, J. Klinowski, M. Forster, A. Lerf, Chem. Phys. Lett. **287**, 53 (1998)
45. Y. Liu, J. Zhou, X. Zhang, Z. Liu, X. Wan, J. Tian, T. Wang, Y. Chen, Carbon **47**, 3113 (2009)
46. D. Yu, Y. Yang, M. Durstock, J.B. Baek, L. Dai, ACS Nano **4**, 5633 (2010)
47. N.M. Huang, H.N. Lim, C.H. Chia, M.A. Yarmo, M.R. Muhamad, Int. J. Nanomed. **6**, 3443 (2011)
48. D. Li, M.B. Mueller, S. Gilje, R.B. Kaner, G.G. Wallace, Nat. Nanotechnol. **3**, 101 (2008)
49. J. Yang, X. Zhao, X. Shan, H. Fan, L. Yang, Y. Zhang, X. Li, J. Alloy. Compd. **556**, 1 (2013)
50. Y. Saito, W. Kubo, T. Kitamura, Y. Wada, S. Yanagida, J. Photochem. Photobiol. A, 164, 153 (2004)
51. S. Siddiqui, P.U. Arumugam, H. Chen, J. Li, M. Meyyappan, ACS Nano **4**, 955 (2010)
52. Q. Cheng, J. Tang, J. Ma, H. Zhang, N. Shinya, L.C. Qin, Carbon **49**, 2917 (2011)
53. W. Gao, S. Cao, Y. Yang, H. Wang, J. Li, Y. Jiang, Thin Solid Films **520**, 6916 (2012)
54. E. Ramasamy, W.J. Lee, D.Y. Lee, J. Song, Electrochem. Commun. **10**, 1087 (2008)